Relaxation time of a quantum RL circuit in the presence of Coulomb interactions

Jianhong He,[1] Wei Liu,[1] Huazhong Guo,[1] and Jie Gao[1,2,*]
[1]*College of Physical Science and Technology, Sichuan University, 610064, Chengdu, China*
[2]*National Institute of Measurement and Testing Technology, 610021, Chengdu, China*

(Received 26 February 2018; revised manuscript received 25 July 2018; published 8 January 2019)

We report on gigahertz admittance measurements indicative of intrinsic relaxation time for an interacting quantum resistance-inductance (RL) circuit formed by a gate-defined quantum point contact in the quantum Hall regime. The dependence of the admittance on intrinsic parameters of the circuit is mapped and found to be highly relevant to the driving frequency, the magnetic field, and the edge potential profile. Remarkably, measurements show that in the coherent limit the relaxation time is universal irrespective of resistance and inductance of the circuit, which is given by the electronic time of flight in the circuit. When the quantum RL circuit is exposed to strong electron interactions, classical laws of electrodynamic response of the whole circuit are recovered, associated with observable variations of relaxation time with resistance. The observed transition of the relaxation time is explained in terms of the effect of Coulomb interaction which is tunable in a gate-defined quantum point contact. Our experiment demonstrates that deviations from the resistance-independent relaxation time are governed by the strength of Coulomb interactions, which provides valuable information to sufficiently determine the interaction parameter.

DOI: 10.1103/PhysRevB.99.045410

I. INTRODUCTION

Quantum coherent electronics for the time-dependent electronic transport in quantum coherent conductors [1] have attracted great interest due to their potential application in quantum information processing [2–6]. A quantum point contact (QPC) [7,8], a short and narrow constriction formed in a high-mobility two-dimensional gas (2DEG), serves as the fundamental building block for manipulating coherent ballistic electronic transport. In QPC systems, many theoretical and experimental investigations have revealed quantum coherent phenomena for the dc transport [9–13] among which quantized conductance is the most quintessential. The ac-transport properties in a QPC, on the other hand, contain rich new physics, especially for the coherent dynamics of charge carriers. The dynamical response of a coherent QPC conductor in electrical isolation has been theoretically addressed [14,15], which can be described in terms of emittance including quantum capacitive and inductive effects, and exhibits dramatic discrepancies with its dc properties. Therefore, the QPC systems can form the basis for the next generation of quantum electronic circuits. Most strikingly, the new quantum circuit based on this QPC system has been realized [16,17], which generates time-resolved single-charge levitons by applying high-frequency Lorentzian voltage pluses. It leads to the possibility of an on-demand anyon source for probing Abelian and non-Abelian anyonic statistics of fractional charges [18].

Of particular interest in dynamical electron transport is the characteristic relaxation time of the quantum circuit which plays a crucial role in characterizing the quantum dynamics of electrons. Recently, a seminal experiment by Gabelli *et al.* [19] in a coherent resistance-capacitance (RC) circuit has demonstrated that the dynamical RC-charge relaxation time, differing from its classical counterparts, is determined by the charge relaxation resistance R_Q independent of the transmission of the QPC [20]. Likewise, the characteristic relaxation time of a chiral quantum resistance-inductance (RL) circuit, given by the ratio of the inductance to the resistance of the circuit, is determined by the time of flight of the electrons transmitting through chiral edge states [21]. As was theoretically predicted [14], the steplike behavior of the QPC emittance is in synchronism with the well-known dc conductance steps, a characteristic signature of quantum coherent transport in an isolated QPC. Essentially, the relaxation time, in the coherent regime, remains constant when the number of propagating modes is varied.

However, a realistic semiconductor 2DEG QPC is formed with the help of gates which introduce an unavoidable coupling of the propagating electron channel to some environmental states. Besides, the emittance is strongly sensitive to the spatial potential distribution inside the QPC, which can be controlled by the external fields. Moreover, Coulomb interactions can cause the emergence of multiple collective modes due to the interchannel coupling [22–24]. These considerable factors lead to electronic decoherence [25,26] and potential fluctuations [27], which trigger a transition of dynamical transport from a quantum coherent to a classical regime, thus provoking a deviation from the constant relaxation time. In previous experimental study [21], the resistance-independent relaxation time of a chiral RL circuit in the absence of Coulomb interaction has been emphasized. Yet, the effects of electron interactions on the relaxation time have been only addressed theoretically in a mesoscopic RL circuit [21] and in a mesoscopic capacitor [28,29]. Therefore, there is demand

*gaojie@scu.edu.cn

for experimentally investigating the impacts of Coulomb interaction on dynamical transport in a quantum RL circuit.

In this paper, we present the study for probing the intrinsic time scales of a quantum RL circuit by measuring the ac admittance of a gate-defined QPC at GHz frequency. We focus exclusively on the L/R relaxation time of an interacting quantum RL circuit. With tuning the magnetic field, the driving frequency, and the gate voltage, we detect the evolution of the L/R time by measuring the dependence of the admittance on intrinsic parameters of the circuit. The resistance-independent relaxation time, associated with the synchronistic stepwise manner for both the real and the imaginary parts of the admittance, is observed only for a frequency-dependent value of the magnetic field in contrast with that observed for different magnetic fields in previous experiments [21]. We find a transition from resistance-independent to classical relaxation time, resulting from Coulomb interactions which are modified by the magnetic field and the gate potential. We employ a current and charge conserving scattering theory extending Ref. [14] to analyze the dynamical conductance of a three-terminal device, which allows us to describe the effect of the gate-mediated interactions. Our measurements demonstrate that the divergence of the L/R time is governed by Coulomb interactions.

II. DEVICES AND MEASUREMENTS

The sample is made in a GaAs/GaAlAs heterostructure with a 2DEG 100 nm below the surface. The 2DEG carrier mobility and density are 2×10^6 cm^2 V^{-1} s^{-1} and 1.4×10^{11}cm^{-2}, respectively. The schematic layout of the device and the measurement setups are presented in Figs. 1(a) and 1(b). The sample size is short enough compared to the wavelength of the edge magnetoplasmon. The two large electron reservoirs, separated by a constriction with a length of $l\sim10\,\mu$m [see Fig. 1(b)], are patterned by wet-etching and optical lithography. A pair of needle-shaped Ti/Au split gates are deposited by electron beam lithography on the middle of the constriction. The length of the gates is $l_g\sim0.5\,\mu$m and their separation is $w\sim0.3\,\mu$m. A QPC is formed by applying negative voltage to the gates. As the gates used in our setup do not cover the whole constriction region ($l_g\ll l$), the interactions are not fully screened, which allows us to probe the effects of Coulomb interactions on dynamical transport. Two low-resistive Au/Ni/Ge ohmic contacts are located at the left and right side of the QPC, and the distance between them is $d\sim80\,\mu$m, which connect to the external circuit via a printed circuit board with two impedance-matched 50 Ω coplanar transmission lines. A constant rf signal is attenuated by the attenuators distributed at different temperature stages, and then applied to left ohmic contact. The output rf signal is amplified by a high-frequency low-noise amplifier and measured by a vector network analyzer Agilent N5244A over a frequency range from 0.8 to 2.2 GHz. As the characteristic impedance Z_0 (= 50 Ω) of the setup is much smaller than the impendence (∼kΩ order) of the device, the admittance can be obtained from the measured scattering matrix element S_{21} as $G(\omega)\sim S_{21}/Z_0$. All measurements have performed in a pulse tube dilution refrigerator Triton 200 with a base temperature of 10 mK and in perpendicular magnetic fields between $B=0$ and 0.5 T.

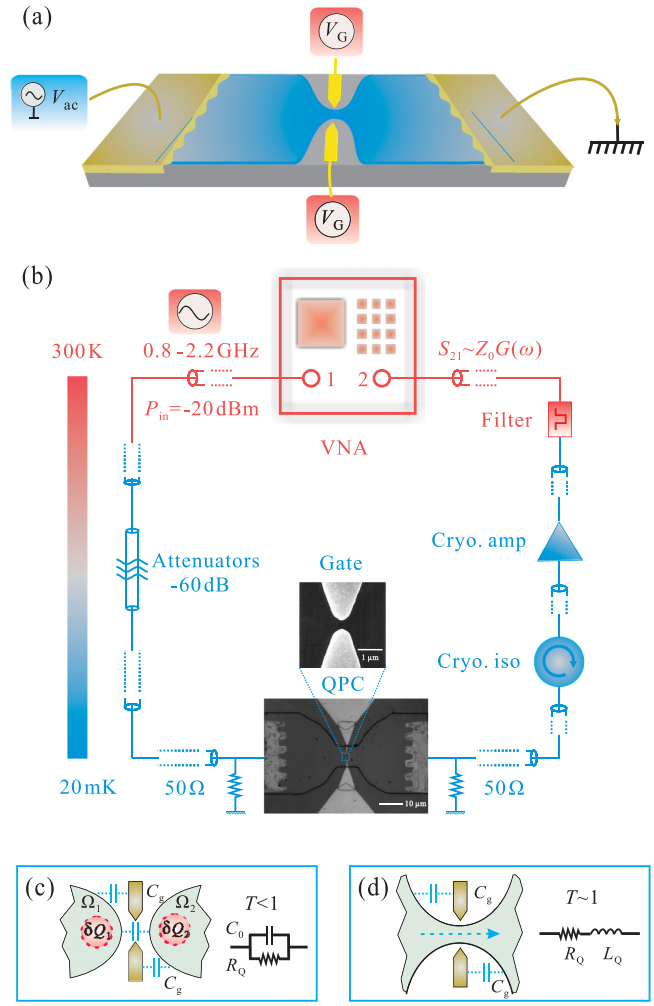

FIG. 1. (a) Views of schematic of the device and measurement setup. (b) The electrical circuit of the admittance measurements based on the optical photography of a whole sample and the electronic photography of the gates. Schematics of the QPC circuit (c) capacitive behavior for the reflected electron modes associated with the dipolar structure of the charge and (d) inductive behavior for the propagating modes through the QPC. C_0 represents the geometric capacitance between the polarized regions Ω_1, Ω_2, and these two regions are equally coupled to the gates with C_g.

III. MODEL

In the low-frequency regime, the admittance $G_{\alpha\beta}(\omega)$ of a phase coherent conductor can be expanded to the first order in frequency [30],

$$G_{\alpha\beta}(\omega)=G^0_{\alpha\beta}-i\omega E_{\alpha\beta}, \tag{1}$$

where $\omega/2\pi$ is the rf driving frequency. The term $G^0_{\alpha\beta}$ has the same form of the dc conductance, $G^0_{\alpha\beta}=(2e^2/h)\mathcal{T}$. Here $\mathcal{T}=n_t+T$ is the sum of the number n_t of the fully transmitted channels and the transmission T of the partially transmitted channel. The first-order term $E_{\alpha\beta}$ is the emittance,

which relates to the displacement charge [14,31] $Q_\alpha = E_{\alpha\beta}V_\beta$, passing through contact α due to a small voltage oscillation $V_\beta \exp(-i\omega t)$ in contact β. The charge Q_α consists of two parts associated with the kinetic contribution $D_{\alpha\beta}V_\beta$ and the screening charge $-\sum_k D^*_{\alpha k}U_k$ induced by the nonequilibrium electric potential U_k, where $D_{\alpha\beta}$ is the global density of states scattered from contact β to α and $D^*_{\alpha k}$ is the partial density of states scattered from region Ω_k to contact α. In the linear response regime, the induced potential U_k is linearly dependent on the potential variation V_β at the contact β, $U_k = \sum_k u_{k_\beta} V_\beta$, and the response coefficients $u_{k\beta}$ are defined as the characteristic potentials [31]. This leads to the emittance matrix:

$$E_{\alpha\beta}(\omega) = e^2\left(D_{\alpha\beta} - \sum_k D^*_{\alpha k}u_{k\beta}\right). \tag{2}$$

In previous theoretical studies [14,15,32], the emittance was expressed in terms of the capacitance and inductance, which can be controlled by the gate voltage of the QPC. More specifically, the negative emittance ($E_{\alpha\beta} < 0$ for $\alpha \neq \beta$), corresponding to the capacitance, is a mesoscopic manifestation of the reflection modes [15]. Whereas the positive emittance ($E_{\alpha\beta} > 0$ for $\alpha \neq \beta$) is an inductive character for mesoscopic conductors with nearly perfect transmission [14], which is determined by the velocities for the transmitted electrons [32]. The emittance changes its sign from negative (capacitive behavior) to positive (inductive behavior) at the certain gate voltage ($T \leqslant 1$) [schematically shown in Figs. 1(c) and 1(d)] taking into account the geometric capacitance, as theoretically predicated in the low-frequency limit [14].

Our starting point is the standard scattering theory for the emittance of the QPC in the presence of the gates extending Ref. [14]. The realistic QPC is formed with the help of the gates, hence it is not in electrical isolation. As the potential of a QPC has the form of a saddle [33], a valley potential is formed away from the saddle point towards the 2DEG [34], which quickly deepens and widens. In contrast to the quantum Hall conductors [30], the polarized regions of Ω_1 and Ω_2 locate immediately in the vicinity of the saddle [Fig. 1(c)] and thus the equilibrium potential and the density of states are nonuniform. In this regime, the charge distribution is not dipolar but consists of three parts Q_1, Q_2, and Q_3 in Ω_1, Ω_2, and at the gates, respectively. Here a symmetric QPC is considered where the two gates are taken to be at the same voltage V_3. Now $E_{\alpha\beta}$ is a three-terminal emittance matrix for the QPC conductor in the presence of gates. The geometric capacitance $C_{0,kj}$ and electrochemical capacitance $C_{\mu,k\beta}$ relate the charge to the induced potential U_j and the variation potential V_β which can be expressed as

$$Q_k = \sum_j C_{0,kj}U_j = \sum_\beta C_{\mu,k\beta}V_\beta. \tag{3}$$

Charge conservation means $Q_1 + Q_2 + Q_3 = 0$. For a single quantum channel, the geometric capacitance matrix can be written,

$$\mathbf{C}_0 = \begin{pmatrix} C_0 + C_g & -C_0 & -C_g \\ -C_0 & C_0 + C_g & -C_g \\ -C_g & -C_g & 2C_g \end{pmatrix}, \tag{4}$$

where C_0 is the geometric capacitance between Ω_1 and Ω_2, and C_g is the geometric capacitance between these regions and the gates. The electrochemical capacitance matrix with capacitance coefficients $C_{\mu,k\beta}$ can be described by

$$\mathbf{C}_\mu = \begin{pmatrix} C_\mu & C_{\mu g} - C_\mu & -C_{\mu g} \\ C_{\mu g} - C_\mu & C_\mu & -C_{\mu g} \\ -C_{\mu g} & -C_{\mu g} & 2C_{\mu g} \end{pmatrix}, \tag{5}$$

where C_μ is the electrochemical capacitance across the QPC and $C_{\mu g}$ is the electrochemical gate capacitance.

The total charges emitted at region Ω_k due to the voltage variation V_β are the sum of the injected charges and the induced negative charges,

$$Q_k = e^2 \sum_{\alpha\beta} D_{\alpha k\beta}(V_\beta - U_k), \tag{6}$$

where $D_{\alpha k\beta}$ is the partial densities of states associated with carriers in Ω_k scattered from contact β at contact α. $D_{\alpha k\beta}$ is given by the transmission probability times the densities of states [32], hence

$$D_{\alpha k\beta} = D_k[\mathcal{T}/2 + \delta_{\alpha\beta}(R\delta_{\alpha k} - \mathcal{T}/2)], \quad \text{if } \alpha, \beta \neq 3. \tag{7}$$

From Eqs. (3) and (6), we can get $u_{k\beta} = (D_{k\beta} - C_{\mu,k\beta})/D_k$, where $D_{k\beta} = \Sigma_\alpha D_{\alpha k\beta}$ corresponds to the partial densities of states associated with carriers injected in contact β. From Eqs. (3)–(7) with the help of the characteristic potentials $u_{k\beta}$, one finds

$$C_{\mu g} = \frac{1}{C_g^{-1} + (NC_q)^{-1}}, \tag{8}$$

$$C_\mu = \frac{(N - \mathcal{T})C_0C_q + (2N - \mathcal{T})(C_g/2)C_q + C_0C_{\mu g}}{NC_q + 2C_0 + C_g}, \tag{9}$$

where N is the filling factor that represents the number of channels around the QPC gate. Using the total density of states $D = 2D_1$ for the symmetric QPC with $D_1 = D_2$. The quantum capacitance is given by $C_q = e^2D_1 = l/v_d$, where l is the propagation length and v_d is the drift velocity. Using the characteristic potential $u_{k\beta}$ and Eqs. (2) and (7) we can calculate the emittance E_{21},

$$E_{21} = \frac{\mathcal{T}^2}{2N^2}(NC_q - \widetilde{C}_{\mu g}) + \frac{\mathcal{T}}{N}\widetilde{C}_{\mu g} - \frac{C_0(NC_q)^2}{(NC_q + C_g)(NC_q + 2C_0 + C_g)}, \tag{10}$$

with

$$\widetilde{C}_{\mu g} = \frac{NC_qC_{\text{geom}}}{NC_q + C_{\text{geom}}}, \tag{11}$$

where C_{geom} is the total geometric capacitance defined as $C_{\text{geom}} = 2C_0 + C_g$. In contrast to the dc conductance independent of the internal potential distribution, the emittance depends sensitively on the fluctuating induced electrical potential [27]. This fluctuating potential emerges in the conductor as a consequence of modification of the charge distribution due to Coulomb interactions. As the gates do not cover the whole interacting region, the interactions, arising from a capacitive coupling between the QPC conductor and

the gates, can be treated as short ranged [35]. In essence, the modification of the charge distribution will substantially affect the dynamical response of the QPC. Therefore, it is necessary to further investigate the dynamical effect of short-range interactions.

We now consider and discuss how interactions qualitatively modify the emittance of the QPC predicated in the standard Büttiker scattering theory [14]. Here we treat the interactions with help of a geometric capacitance $C_{\rm geom}$ in the random-phase approximation (RPA) [1,35–37] and the gate as a macroscopic conductor with on dynamics of its own. For this case, the modification of the charge distribution on the conductor is $\delta\hat{Q} = C_{\rm geom}\delta\hat{U}(\omega)$, which is the sum of the bare charge fluctuations $e\hat{\mathcal{N}}(\omega)$ and the induced charges generated by the fluctuating induced internal potential $\delta\hat{U}(\omega)$ [37]. In the RPA, the induced charges $\delta\hat{Q}_{\rm ind}$ are directly related to the average frequency-dependent density of states $D(\omega)$ and the fluctuating potential $\delta\hat{U}(\omega)$, which is determined by $\delta\hat{Q}_{\rm ind} = -e^2ND(\omega)\delta\hat{U}(\omega)$. Thus, the modification of the charge is given by

$$\delta\hat{Q} = C_{\rm geom}\delta\hat{U}(\omega) = e\hat{\mathcal{N}}(\omega) - e^2ND(\omega)\delta\hat{U}(\omega). \quad (12)$$

The operator of the potential fluctuations $\delta\hat{U}(\omega)$ can be obtained by solving this equation as

$$\delta\hat{U}(\omega) = F(\omega)e\hat{\mathcal{N}}(\omega), \quad (13)$$

with

$$F(\omega) = [C_{\rm geom} + e^2ND(\omega)]^{-1}. \quad (14)$$

Worthy of note here is that $F(\omega)$ takes into consideration the effective interaction potential. Consequently, the frequency-dependent quantum capacitance is $C_{\rm q}(\omega) = e^2D(\omega)$, defined as [38]

$$C_{\rm q}(\omega) = iC_{\rm q}\frac{1-\exp(i\omega\tau_{\rm t})}{\omega\tau_{\rm t}}. \quad (15)$$

Here $\tau_{\rm t}$ is the traversal time that an electron spends passing through the interacting region. As follows from Eq. (15), the correction to the electrochemical gate capacitance given by Eq. (11), is relevant to the driving frequency, which then takes the form as $\widetilde{C}_{\mu\rm g}(\omega) = F(\omega)NC_{\rm q}(\omega)C_{\rm geom}$. In this respect, the emittance [Eq. (10)] can no longer be regarded as a frequency-independent function.

One can find from Eq. (10) that the emittance E_{21} of the generalization QPC system is the nonlinear function containing a quadratic term. When all transport channels are closed ($\mathcal{T} = 0$), the QPC behaves like a capacitor. Thus, the third constant term in Eq. (10) corresponds to the purely capacitive emittance which can be subtracted at experimental calibration process and allows one to focus on the inductive admittance of the QPC at finite transmission. Namely, the admittance of a QPC conductor can be described by a resistance R ($R = 1/G^0_{\alpha\beta}$) in series with an inductance L, schematically shown in Fig. 1(d). The L/R relaxation time $\tau_{RL} = -{\rm Im}(G)/\omega{\rm Re}(G)$ is then given by

$$\tau_{RL} = \frac{h}{2e^2}\left[\frac{\mathcal{T}}{2N^2}(NC_{\rm q}(\omega) - \widetilde{C}_{\mu\rm g}(\omega)) + \frac{\widetilde{C}_{\mu\rm g}(\omega)}{N}\right]. \quad (16)$$

Note that here τ_{RL} is frequency dependent, which is a relevant time scale characterizing the dynamical response of the QPC system. It consists of two terms: The first one is a linear dependence on $\mathcal{T}$, simplified as $A_1\mathcal{T}$, while the second one is transmission independent, simplified as A_0. Therefore, τ_{RL} can be simplified as $\tau_{RL} = A_1\mathcal{T} + A_0$. It is important to note that the ratio of the two coefficients is fully determined by the capacitances as $K = A_1/A_0 = C_{\rm q}(\omega)/2C_{\rm geom}$, which encodes the effect of Coulomb interaction. Electronic transport in a quasi-one-dimensional QPC system with short-range interactions is well described by Luttinger liquid theory [39,40]. The interaction (Luttinger) parameter g, determining the amount of screening and the strength of the effective Coulomb interaction, is related to the density of states and the geometric capacitance via $g^2 = 1/(1 + e^2D(\omega)/C_{\rm geom})$ [35], which gives $K = (1-g^2)/2g^2$. As the density of states significantly depends on the frequency and the magnetic field, the interactions can be modified by adjusting them in the circuit. Namely, the quantum capacitance [Eq. (15)] can be suppressed relative to the geometric capacitance upon increasing the frequency, which allows for probing the effect of frequency-dependent screening [25]. At a finite frequency, for $C_{\rm q} \ll C_{\rm geom}$, so that $g \to 1$ and $K \to 0$, the Coulomb energy $e^2/2C_{\rm geom}$ goes to zero that the interactions are effectively screened. This means that the electrons travel ballistically along one-dimensional channels located at the edge of the sample. The charge behaves like a free noninteracting particle. The relaxation time reduces to $\tau_{RL} = (h/2e^2)\widetilde{C}_{\mu\rm g}/N$ which is transmission independent, predicting the synchronistic stepwise manner of both the real and imaginary parts of the admittance at the opening of the QPC channels. For $C_{\rm geom} \ll C_{\rm q}$, $g \to 0$, and $K \gg 1$, the strength of the electron interactions is increased, which leads to $\tau_{RL} = (h/2e^2)(\mathcal{T}/2N^2)(NC_{\rm q} - \widetilde{C}_{\mu\rm g})$. The classical laws are recovered, i.e., the inductance $L = (h/2e^2)^2(NC_{\rm q} - \widetilde{C}_{\mu\rm g})/2N^2$ does not vary when the resistance $1/G^0_{\alpha\beta}$ is modified.

IV. RESULTS AND DISCUSSION

A. The admittance of a QPC in the presence of gates

We first turn to the admittance measurements and demonstrate how the inductive admittance is differentiated from the capacitive admittance of a QPC. Figure 2(a) shows the variation of the phase $\Delta\varphi(V_{\rm G})$ of the ac admittance relative to the pinch-off point, $\Delta\varphi(V_{\rm G}) = \varphi(V_{\rm G}) - \varphi(V_{\rm pin-off})$, as a function of the gate voltage $V_{\rm G}$ at various magnetic fields. As can be seen from Fig. 2(a), the phase jump $\Delta\varphi_{0\to1}$ for the first step increases with increasing magnetic field. This can be understood from the dominant contribution between the kinetic part and the screening part to the emittance. It is intuitively obvious that the kinetic contribution increases which arises from the reduction of the drift velocity of the transmitted electrons with increasing magnetic field, but no influence on the reflected electron modes. Thus, the capacitive-inductive transition point moves toward negative gate voltage corresponding to smaller transmission due to the increasing of the inductance contribution as the magnetic field increases at a fixed frequency. Figures 2(c) and 2(d) show the phase of the admittance as a function of $V_{\rm G}$ for different frequencies at $B = 0$ and 0.2 T, respectively. We find that the location

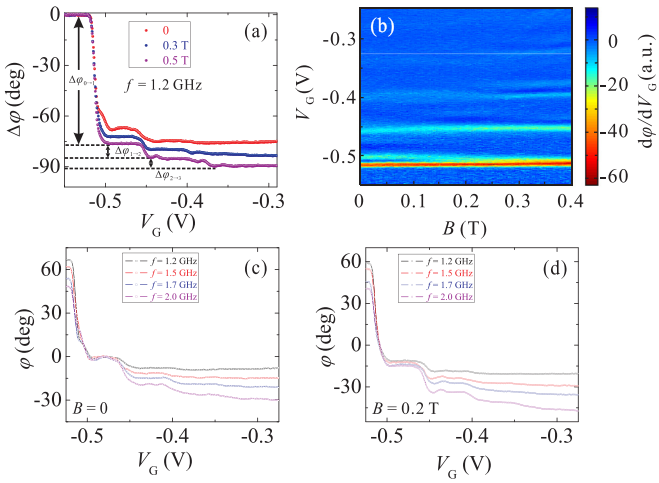

FIG. 2. (a) Phase variations $\Delta\varphi(V_{\rm G})$ of the admittance measured from the pinch-off of the gate voltage, $\Delta\varphi(V_{\rm G}) = \varphi(V_{\rm G}) - \varphi(V_{\rm pin-off})$, as a function of $V_{\rm G}$ for various magnetic field at $f = 1.2$ GHz. (b) Numerical derivative $d\varphi/dV_{\rm G}$ of the phase of the admittance with respect to B and $V_{\rm G}$. Phase of the admittance for various frequencies at (c) $B = 0$ and (d) $B = 0.2$ T, respectively.

of the capacitive-inductive transition point is independent of the driving frequency, which is consistent with the previous theoretical results [15,41]. Another important phenomenon shown in Fig. 2(a), dictates that the first phase jump $\Delta\varphi_{0\to1}$ changes more rapidly than the subsequent one $\Delta\varphi_{m\to n}$ at the opening of the QPC, that is, $\Delta\varphi_{0\to1} \gg \Delta\varphi_{m\to n}$ $(n > m \geqslant 1)$, which is further verified in the color-scale plot of the numerical derivative of the phase $d\varphi/dV_{\rm G}$ [Fig. 2(b)]. It implies that the QPC has an inductive character due to the predominant role of the open channels ($n_{\rm t} > 1$), and the capacitive behavior is mainly determined by the nonpropagating modes for $n_{\rm t} = 0$ or 1. This allows us to subtract the capacitive admittance before the zero transition point and focus on the evolution characteristics of inductive admittance at finite transmission.

We now study the dependence of the admittance on the relevant parameters such as the magnetic field, the driving frequency, and the gate voltage. Figures 3(a) and 3(b) show the real and imaginary parts of the admittance [Re(G) and Im(G)] as a function of $V_{\rm G}$ for five different magnetic fields at $f = 2.0$ GHz and 1.5 GHz, respectively. Both the Re(G) and Im(G) exhibit similar stepwise structure as the number of open channels increases by changing the transmission of the QPC. Note that Im(G) is negative, and the height of its step is proportional to the driving frequency. It reflects the fact that the measured current flowing across the QPC is delayed relative to the applied ac voltage due to the inductive contribution of the emittance. The number of plateaus decreases upon increasing the magnetic field at the fixed gate voltage range (-0.55 V $< V_{\rm G} < -0.25$ V). It indicates that the number of the opening subbands decreases, which results from the increasing energy splitting of subbands. On the other hand, the plateaus of both Re(G) and Im(G) become more flat and synchronous at a specific magnetic field, marked by red dotted curves in Figs. 3(a) and 3(b), while Im(G) and Re(G) are no longer strictly mutual proportional for other magnetic fields and have relatively larger fluctuations. It signals a possible transition, and indicates that the admittance of a QPC in the presence of gates is sensitive to the magnetic field and the gate potential.

These features can be most directly depicted in Nyquist representations, i.e., Im(G) as a function of Re(G) [Figs. 3(c) and 3(d)], which show that the phase of the admittance evolves as the magnetic field and the gate voltage. Contrasted with the previous experiments in a two-terminal quantum Hall device [21], the transmission-independent phase of the admittance of the gate-defined QPC conductor is observed only for a critical magnetic field defined as $B_{\rm CO}$. Note that it relates to the driving frequency as a higher frequency corresponds to a smaller magnetic field $B_{\rm CO}$ [see Figs. 3(c) and 3(d)]. Below and above this field $B_{\rm CO}$, the variations of Im(G) versus Re(G) follow a quadratic but with opposite concavities when sweeping the gate voltage of the QPC, which are concave upward for $B < B_{\rm CO}$ and concave downward for $B > B_{\rm CO}$. It signals the presence of a transition of the relaxation time, $\tau_{RL} = -{\rm Im}(G)/\omega{\rm Re}(G)$, from resistance-independent to classical L/R time. We argue that this behavior results from both Coulomb interactions [42–44] between the propagating electron edge channels and their coupling to surrounding gates [27], which were not included in previous experimental study [21] as they are efficiently screened on a quantum Hall bar by a pair of large side gates.

The concavity-convexity of Im(G) versus Re(G) is directly related to the interaction strength $|1 - g^2|$ (i.e., detuned from the noninteracting value 1), which can be measured in terms of the dimensionless parameter $K = e^2 D(\omega)/2C_{\rm geom}$, as already defined above. Figures 3(e) and 3(f) show K as a function of B extracted from the quadratic fits of the data in Figs. 3(c) and 3(d), respectively. The data agree qualitatively with the expected linear B dependence of K [i.e., $D(\omega) \propto B$] but with different slope ratio in different magnetic field ranges, showing that, upon increasing the magnetic field, the convexity sharply enhances in the range of $B > B_{\rm CO}$ and the concavity slowly weakens in the range of $B < B_{\rm CO}$. This asymmetric evolution is a direct consequence of the variations of the local density of states $D(\omega)$ relative to the geometric capacitance accounting for modifications of electron-electron interactions by tuning the magnetic field and the driving frequency.

For $B < B_{\rm CO}$, electronic propagating modes correspond to magnetoelectric subbands interacting into the edges of the constriction [45,46], accordingly, that electron-electron interactions are mainly mediated by boundary scattering [47,48]. These interactions are related to electronic exchange and correlations [49], giving a possible explanation for the measured negative value of the nontrivial factor $K \lesssim 0$. They can be described by an additional capacitance $C_{\rm xc}$, which is expected to be negative at low densities and crosses over to positive values at higher densities [49–51]. Thus, whenever opening a new subband, it adds a new negative $C_{\rm xc}$ in series with $C_{\rm q}$ and $C_{\rm geom}$. As $C_{\rm q}$ is given by the density of states, $C_{\rm xc}$ can be regarded as a correction to the geometric capacitance, $\widetilde{C}_{\rm geom} = C_{\rm geom}(1 + \chi)^{-1}$, thereby $\widetilde{K} = (1 + \chi)K$, where χ is the capacitance ratio $C_{\rm geom}/C_{\rm xc}$. As shown in Fig. 3(f), the negative K increases due to the increase of the density states in the range of $0 \leqslant B \leqslant B_{\rm CO}$ (=0.24 T), corresponding to

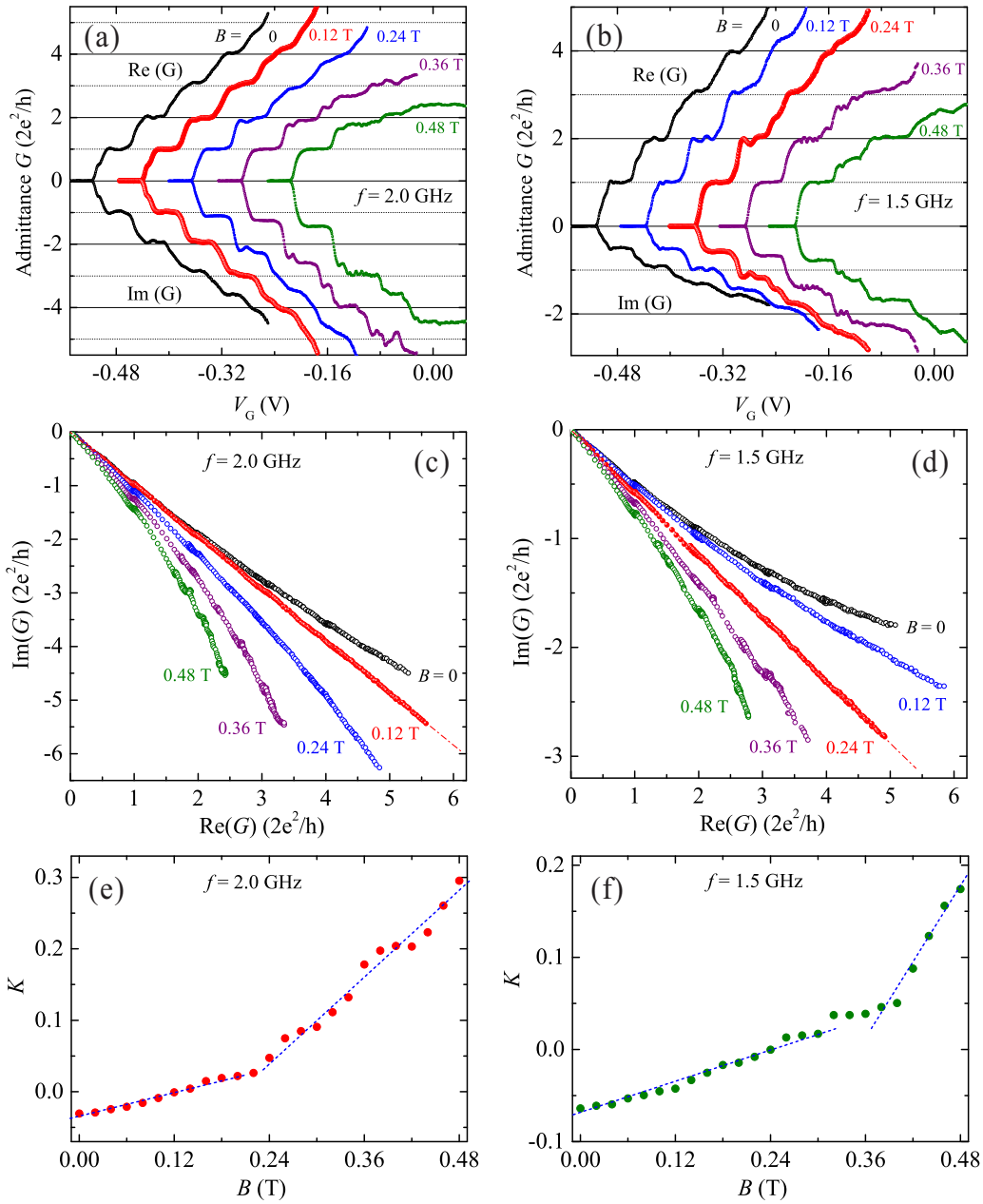

FIG. 3. Re(G) (upper half) and Im(G) (bottom half) of the admittance as a function of V_G for five different magnetic fields at (a) $f = 2.0$ GHz and (b) $f = 1.5$ GHz, respectively. The curves of nonzero magnetic fields are shifted along V_G axis by steps of 0.15 V for better visibility. (c) and (d) The corresponding Nyquist representations of the admittance data in (a) and (b), respectively. Red dashed dotted lines show linear fits to the data, $\mathrm{Im}(G) \propto \mathrm{Re}(G)$, at $B = 0.12$ T for $f = 2.0$ GHz and $B = 0.24$ T for $f = 1.5$ GHz. (e) and (f) The interaction strength K as a function of B deduced from the quadratic fits of the data in (c) and (d), respectively. The blue short dashed lines present linear fits to the data, $K \propto B$. The slope of the fitted lines in range of $B > B_{\mathrm{CO}}$ is much larger than that in range of $B < B_{\mathrm{CO}}$; see text in detail.

$-0.16 \leqslant 1 - g^2 \leqslant 0$. Similar behavior is observed for $f = 2.0$ GHz in Fig. 3(e) with $-0.07 \leqslant 1 - g^2 \leqslant 0$. This quantitative difference may originate from the enhanced screening effect at high frequency [38], which will be discussed in the following section. As the magnetic field further increases, electronic propagating modes gradually evolve into chiral edge states surrounding an incompressible bulk [45]. The widths and positions of these edge and bulk configurations vary with the magnetic field, resulting in the modification of C_g and C_0 (i.e., C_{geom}), and thus the interchannel Coulomb interaction strength [52]. When the magnetic field is increased, the channels move apart from the gates, thereby reducing C_{geom} and increasing $D(\omega)$ simultaneously. Consequently, the steep enhancement of K in the range of $B > B_{\mathrm{CO}}$ [see Figs. 3(e) and 3(f)] indicates the interaction strength $(1 - g^2) \geqslant 0$ that changes rapidly in this B range.

Noteworthily, Figs. 3(c) and 3(d) also dictate that, at a fixed magnetic field and gate voltage, the relaxation time is strongly sensitive to the driving frequency, consistent with the above prediction in consideration of the potential fluctuations induced by boundary-mediated interactions. For instance, at $B = 0.12$ T, a linear Re(G) dependence of Im(G) is ob-

served for $f = 2.0$ GHz, meaning that the relaxation time is resistance independent upon varying the gate voltage. While for $f = 1.5$ GHz, the dependence of $\mathrm{Im}(G)$ on $\mathrm{Re}(G)$ is no longer linear, namely, the relaxation time becomes resistance dependent. It indicates that the driving frequency plays a crucial role on the dynamics of electrons in the circuit. This observation for $B < B_{\mathrm{CO}}$ can be understood in terms of the frequency-dependent screening effect for boundary scattering, which significantly enhances with an increase of the frequency at a fixed magnetic field, similar to what has been observed in Ref. [25]. In contrast, for $B > B_{\mathrm{CO}}$, in spite of the interaction-induced boundary scattering being relatively weak, interband inelastic scattering is significantly strengthened. In this regime, increasing the driving frequency f increases the available energy for inelastic scattering, thus enhancing interaction effects. Consequently, the concavity strongly enhances when the frequency is increased, e.g., for $B = 0.48$ T as shown in Figs. 3(c) and 3(d). We will study hereafter the nature of the relaxation time extracted from the measured admittance of the QPC upon varying the intrinsic parameters of the circuit, and demonstrate that the divergence of the relaxation time is indeed due to Coulomb interactions.

B. The resistance-independent relaxation time τ^{c}_{RL}

Considering that the interactions significantly depend on both the driving frequency and the magnetic field, and thus we can tune them, i.e., suppress the quantum capacitance with respect to the geometric capacitance, for observation of the resistance-independent relaxation time τ^{c}_{RL} with $g^2 = 1$. In Fig. 4(a), we plot the curves with a linear $\mathrm{Re}(G)$ dependence of $\mathrm{Im}(G)$ choosing for different driving frequencies at their corresponding magnetic field B_{CO}. These correspond to the noninteracting case with a resistance-independent relaxation time, as expected, for which the interaction parameter $g^2 \approx 1$ is extracted from the linear fits in Fig. 4(a). For $g^2 = 1$, the relaxation time reduces to $\tau^{\mathrm{c}}_{RL} = (h/2e^2)\widetilde{C}_{\mu\mathrm{g}}(\omega)/N$. Remarkably, when the term $\widetilde{C}_{\mu\mathrm{g}}(\omega)/N$ turns to be constant by varying the driving frequency together with tuning the magnetic field, the relaxation time τ^{c}_{RL} becomes universal. As a result, the phase of the admittance draws a straight line in Fig. 4(b) with a linear ω dependence of the phase, $\tan(\phi) = -\omega\tau^{\mathrm{c}}_{RL} \propto \omega$.

In this noninteracting limit, the relaxation time τ^{c}_{RL} is in striking contrast with the time constant $[L/R \propto \mathrm{Re}(G)]$ of a classical circuit. Such a violation of classical laws has been demonstrated that it requires a coherent chiral propagation of electrons enforced by a magnetic field [21]. As Fig. 4(c) shows, the required magnetic field B_{CO}, accounting for transmission-independent phase factors [Fig. 4(a)], decreases with the increase of the driving frequency. This reflects the intrinsic dynamical characteristics of a coherent RL circuit. In the ac transport, it is necessary to consider two parts of the current which includes the particle current $I_{\mathrm{p}}(\omega)$ and the displacement current $I_{\mathrm{d}}(\omega)$. In the limit of ballistic transport in a quasi-one-dimensional channel, the particle current $I_{\mathrm{p}}(\omega)$ is primarily determined by the drift velocity v_{d} of the transmitted electrons as $I_{\mathrm{p}}(\omega) \propto n_e e v_{\mathrm{d}}$, and the total carrier density in the transmitted channel can be estimated by using the simple capacitance relation $n_e = C_{\mathrm{geom}}\Delta V_{\mathrm{G}}/el$, where ΔV_{G} is the gate voltage measured from pinch-off. The displacement current

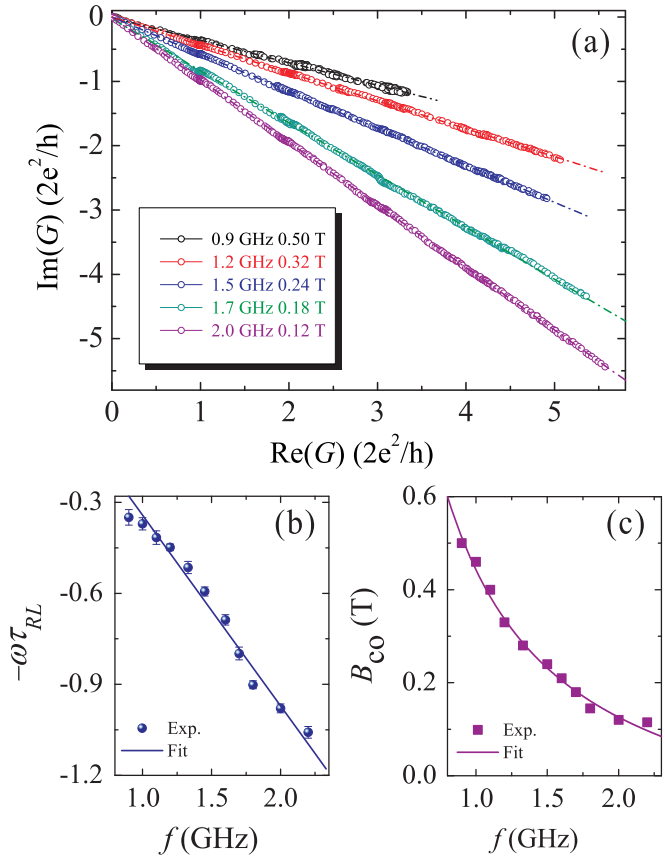

FIG. 4. (a) Characteristic linear Nyquist diagram of the admittance [$\mathrm{Im}(G)$ as a function of $\mathrm{Re}(G)$] for different frequencies at their corresponding critical values of the magnetic field B_{CO}. The dashed dotted lines show linear fits to the data. (b) Frequency dependence of the phase of the admittance in (a). The blue line is fit to the data, $\tan(\phi) = -\omega\tau_{RL} \propto f$. (c) Dependence of the required magnetic field B_{CO} on the driving frequency. The purple solid line is fit to the data, $B_{\mathrm{CO}} \propto f^{-1}$.

$I_{\mathrm{d}}(\omega)$ related to the induced potential $U(\omega)$ is proportional to frequency. According to Eq. (3), it can be expressed as $I_{\mathrm{d}}(\omega) = -i\omega C_0 U(\omega)$. To recover current conservation, they should satisfy the condition $I(\omega) \equiv I_p(\omega) = I_{\mathrm{d}}(\omega)$ [14]. As the drift velocity v_{d} is inversely proportional to the magnetic field, one can find $B_{\mathrm{CO}} \propto f^{-1}$. Consequently, the case for relatively higher frequency requires a much lower magnetic field to compensate the screening effect. This essentially means that, when the frequency-dependent screening enhances upon increasing the driving frequency, the suppression of the interactions created exclusively by the magnetic field reduces accordingly.

The resistance-independent relaxation time τ^{c}_{RL} of a coherent RL circuit is indeed directly related to the electronic dwell time $\tau_{\mathrm{d}} = l/v_{\mathrm{c}}$ in the circuit, characteristic of the noninteracting system ($g^2 = 1$) [53]. Note that here $v_{\mathrm{c}} = v_{\mathrm{d}} + 2e^2 Nl/hC_{\mathrm{geom}}$ is the drift velocity renormalized by the screened Coulomb interaction. From $\tau_{\mathrm{d}} = \tau^{\mathrm{c}}_{RL} = 0.07 \pm 0.015$ ns extracted from the linear fits in Fig. 4(b), and the estimated propagation length $l \approx 10\,\mu$m [the length of the constriction region in Fig. 1(b)], we obtain a drift velocity $v_{\mathrm{c}} \approx 10^5$ m/s in this noninteracting limit. It is in agreement

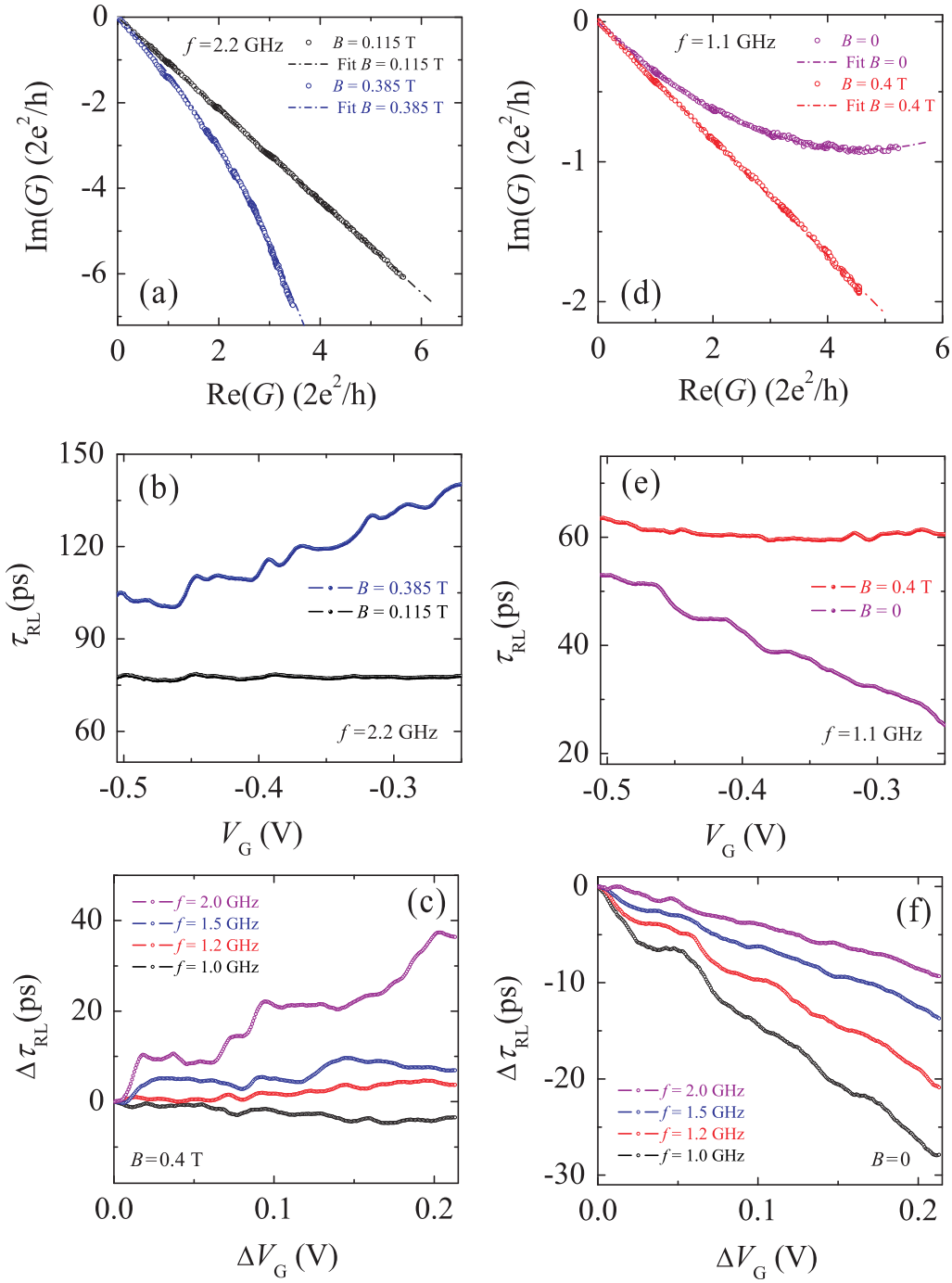

FIG. 5. (a) Nyquist representation of the admittance at $B = 0.115$ T and 0.385 T for the frequency $f = 2.2$ GHz. (b) The relaxation time τ_{RL} as a function of V_G for data in (a). Variations of the relaxation time $\Delta\tau_{RL}$ as a function of ΔV_G for four different frequencies at (c) $B = 0.4$ T and (f) $B = 0$, respectively. (d) Nyquist representation at $B = 0$ and 0.4 T for the frequency $f = 1.1$ GHz. (e) The relaxation time τ_{RL} as a function of V_G for the data in (d). The black and red dashed dotted lines are fits to the data, Im(G) $\propto$ Re(G). The blue and purple dashed lines represent the curve fits with quadratic function, $\mathrm{Im}(G) = A_1[\mathrm{Re}(G)]^2 + A_0\mathrm{Re}(G)$.

with the result for the noninteracting case in the previous study [21]. On the other hand, with this relation Eq. (16) can be rewritten in a more convenient form as

$$\tau_{RL} = \tau_d(1 + K\mathcal{T}). \tag{17}$$

As already mentioned, the nontrivial factor $K = (1 - g^2)/2g^2$ is a sensitive function of the interaction strength, which evaluates the deviation from the resistance-independent relaxation time τ_d.

C. The divergence of the L/R relaxation time

In Fig. 5(a), we show the Nyquist diagram of the admittance for the frequency $f = 2.2$ GHz at the magnetic fields $B = B_{CO} = 0.115$ T and 0.385 T. At $B > B_{CO}$, the variations

of $\mathrm{Im}(G)$ versus $\mathrm{Re}(G)$ follow a quadratic law with concave downward, indicating that the relaxation time is resistance dependent. The fundamental parameters K and g^2 are obtained through a quadratic polynomial fitting, which gives $K = 0.22$ and $g^2 = 0.69$. In contrast to $K \approx 0$ and $g^2 \approx 1$ for the noninteracting case at $B = B_{\mathrm{CO}}$, this value $g^2 < 1$ corresponds to repulsive Coulomb interactions [40,54]. It confirms that the positive deviation from the resistance-independent relaxation time results from the interedge Coulomb interactions which strongly enhance due to the increasing of the density of states upon increasing the magnetic field. On the other hand, it reflects the fact that electrons slow down passing through the interacting region of the QPC since the drift velocity of an electron is inversely proportional to the density of states, $D(\omega) \propto v_{\mathrm{d}}^{-1}$. The slow electrons undergo strongly enhanced interactions, thus effectively lengthening the QPC time of flight [55]. As a consequence, the relaxation time τ_{RL} is much larger than the constant time τ_{RL}^{c} at $B = B_{\mathrm{CO}}$, as shown in Fig. 5(b), and their difference significantly increases upon opening more subbands of the QPC. In Fig. 5(c), we plot the variation of the relaxation time $\Delta\tau_{RL}$ as a function of ΔV_{G} for four different frequencies, where ΔV_{G} is the gate voltage measured from pinch-off. Clearly, $\Delta\tau_{RL} > 0$ at $B > B_{\mathrm{CO}}$, and it increases upon increasing the frequency and lowering the gate potential at a finite magnetic field. This implies that if $\tau_{RL} > \tau_{RL}^{c}$ electronic transport in an interacting channel decoheres before the transmitted electrons flow into the contact. This is confirmed by the emergence of the larger fluctuations of the relaxation time, notably, when a new subband opens [see Figs. 5(b) and 5(c)]. It results from interband inelastic scattering induced by the electron interactions, which demolishes the coherent transport [26,56].

By contrast, we plot in Fig. 5(d) the Nyqusit diagrams of the admittance for a low frequency of $f = 1.1$ GHz at zero magnetic field and $B = B_{\mathrm{CO}} = 0.4$ T. This low frequency is chosen so that the frequency-dependent screening effect is relatively weak, namely, the boundary-mediated interaction effect is significantly strong, which is convenient for observation of significant deviations from the constant relaxation time at $B < B_{\mathrm{CO}}$. At zero magnetic field, the variations of $\mathrm{Im}(G)$ versus $\mathrm{Re}(G)$ follow an expected quadratic law but with concave upward. For this case, $K = -0.1$ and $g^2 = 1.28$ are extracted from the quadratic polynomial fitting [Fig. 5(d)]. For $K \lesssim 0$ and $g^2 > 1$, the boundary-mediated interactions can reduce the emittance of the QPC via scattering of emitted electrons back to the QPC [57]. Thus, when the gate voltage is increased, the relaxation time, $E/\mathrm{Re}(G)$, rapidly decreases that compared with the noninteracting case ($g^2 = 1$ at $B = B_{\mathrm{CO}}$), as shown in Fig. 5(e). Although qualitatively similar, this behavior is found to be more pronounced at the lower frequency; see Fig. 5(f). This is consistent with the frequency-dependent interaction effects, which should have, in principle, an enhanced screening effect at high frequencies when the system resembles Luttinger liquid with boundary-mediated electron interactions [47,48]. In general, for the noninteracting case $g^2 = 1$, the relaxation time is constant regardless of resistance and inductance of the circuit which can be realized by tuning the magnetic field and the gate potential. For all $g^2 \neq 1$, deviations from the constant relaxation time as a function of transmission probabilities are governed by the strength of electron interactions [54].

V. CONCLUSION

In conclusion, we have measured gigahertz admittance of a QPC in the presence of gates, indicative of intrinsic relaxation time for an interacting quantum RL circuit. The transmission-independent phase of the admittance, i.e., $\mathrm{Im}(G) \propto \mathrm{Re}(G)$, is observed only for a critical magnetic field B_{CO} dependent on the driving frequency, in contrast with that observed for different magnetic fields in a completely screened Hall system [21]. Deviating from this critical field B_{CO}, the variations of $\mathrm{Im}(G)$ versus $\mathrm{Re}(G)$ follow a quadratic law but with opposite concavities, which is governed by the strength of Coulomb interactions. Our observations clarify that phase-coherent dynamical transport in a gate-defined QPC is characterized by the synchronic stepwise manner for both the conduction and the emittance, associated with the relaxation time regardless of resistance and inductance of the circuit. We find that the relaxation time deviates from the resistance-independent time and even turns to classical L/R time in the presence of strong electron interactions. Our work provides a dynamical means to evaluate the effects of Coulomb interaction on the basis of the relaxation time measurement, and may have impact on fundamental studies of dynamical quantum transport in mesoscopic Coulomb-coupled conductors.

ACKNOWLEDGMENTS

This research was supported by the National Key R&D Program of China under Grant No. 2016YFF0200403 and the Key Program of National Natural Science Foundation of China under Grant No. 11234009.

[1] M. Büttiker, A. Prêtre, and H. Thomas, Phys. Rev. Lett. **70**, 4114 (1993).
[2] E. Bocquillon, V. Freulon, J.-M. Berroir, P. Degiovanni, B. Plaçais, A. Cavanna, Y. Jin, and G. Fève, Science **339**, 1054 (2013).
[3] D. Dasenbrook and C. Flindt, Phys. Rev. Lett. **117**, 146801 (2016).
[4] B. Gaury and X. Waintal, Nat. Commun. **5**, 3844 (2014).
[5] D. Kim, D. R. Ward, C. B. Simmons, J. K. Gamble, R. Blume-Kohout, E. Nielsen, D. E. Savage, M. G. Lagally, M. Friesen, S. N. Coppersmith, and M. A. Eriksson, Nat. Nanotechnol. **10**, 243 (2015).
[6] Z. V. Penfold-Fitch, F. Sfigakis, and M. R. Buitelaar, Phys. Rev. Applied **7**, 054017 (2017).
[7] B. J. van Wees, H. van Houten, C. W. J. Beenakker, J. G. Williamson, L. P. Kouwenhoven, D. van der Marel, and C. T. Foxon, Phys. Rev. Lett. **60**, 848 (1988).
[8] D. A. Wharam, T. J. Thornton, R. Newbury, M. Pepper, H. Ahmed, J. E. F. Frost, D. G. Hasko, D. C. Peacockt, D. A. Ritchie, and G. A. C. Jones, J. Phys. C **21**, L209 (1988).

[9] R. Crook, J. Prance, K. J. Thomas, S. J. Chorley, I. Farrer, D. A. Ritchie, M. Pepper, and C. G. Smith, Science **312**, 1359 (2006).

[10] M. J. Iqbal, R. Levy, E. J. Koop, J. B. Dekker, J. P. de Jong, J. H. M. van der Velde, D. Reuter, A. D. Wieck, R. Aguado, Y. Meir, and C. H. van der Wal, Nature (London) **501**, 79 (2013).

[11] F. Bauer, J. Heyder, E. Schubert, D. Borowsky, D. Taubert, B. Bruognolo, D. Schuh, W. Wegscheider, J. von Delft, and S. Ludwig, Nature (London) **501**, 73 (2013).

[12] S. Maeda, S. Miyamoto, M. H. Fauzi, K. Nagase, K. Sato, and Y. Hirayama, Appl. Phys. Lett. **109**, 143509 (2016).

[13] C. Yan, S. Kumar, M. Pepper, P. See, I. Farrer, D. Ritchie, J. Griffiths, and G. Jones, Phys. Rev. Applied **8**, 024009 (2017).

[14] T. Christen and M. Büttiker, Phys. Rev. Lett. **77**, 143 (1996).

[15] I. E. Aronov, N. N. Beletskii, G. P. Berman, D. K. Campbell, G. D. Doolen, and S. V. Dudiy, Phys. Rev. B **58**, 9894 (1998).

[16] J. Dubois, T. Jullien, F. Portier, P. Roche, A. Cavanna, Y. Jin, W. Wegscheider, P. Roulleau, and D. C. Glattli, Nature (London) **502**, 659 (2013).

[17] T. Jullien, P. Roulleau, B. Roche, A. Cavanna, Y. Jin, and D. C. Glattli, Nature (London) **514**, 603 (2014).

[18] D. C. Glattli and P. S. Roulleau, Phys. Status Solidi B **254**, 1600650 (2017).

[19] J. Gabelli, G. Fève, J.-M. Berroir, B. Plaçais, A. Cavanna, B. Etienne, Y. Jin, and D. C. Glattli, Science **313**, 499 (2006).

[20] M. Büttiker, H. Thomas, and A. Prêtre, Phys. Lett. A **180**, 364 (1993).

[21] J. Gabelli, G. Fève, T. Kontos, J.-M. Berroir, B. Plaçais, D. C. Glattli, B. Etienne, Y. Jin, and M. Büttiker, Phys. Rev. Lett. **98**, 166806 (2007).

[22] M. Kataoka, N. Johnson, C. Emary, P. See, J. P. Griffiths, G. A. C. Jones, I. Farrer, D. A. Ritchie, M. Pepper, and T. J. B. M. Janssen, Phys. Rev. Lett. **116**, 126803 (2016).

[23] P. Degiovanni, Ch. Grenier, and G. Fève, Phys. Rev. B **80**, R241307 (2009).

[24] A. Marguerite, C. Cabart, C. Wahl, B. Roussel, V. Freulon, D. Ferraro, Ch. Grenier, J.-M. Berroir, B. Plaçais, T. Jonckheere, J. Rech, T. Martin, P. Degiovanni, A. Cavanna, Y. Jin, and G. Fève, Phys. Rev. B **94**, 115311 (2016).

[25] E. Bocquillon, V. Freulon, J.-M. Berroir, P. Degiovanni, B. Plaçais, A. Cavanna, Y. Jin, and G. Fève, Nat. Commun. **4**, 1839 (2013).

[26] V. Freulon, A. Marguerite, J.-M. Berroir, B. Plaçais, A. Cavanna, Y. Jin, and G. Fève, Nat. Commun. **6**, 6854 (2015).

[27] C. Altimiras, F. Portier, and P. Joyez, Phys. Rev. X **6**, 031002 (2016).

[28] S. E. Nigg and M. Büttiker, Phys. Rev. B **77**, 085312 (2008).

[29] Y. Hamamoto, T. Jonckheere, T. Kato, and T. Martin, Phys. Rev. B **81**, 153305 (2010).

[30] T. Christen and M. Büttiker, Phys. Rev. B **53**, 2064 (1996).

[31] M. Büttiker, J. Phys.: Condens. Matter **5**, 9361 (1993).

[32] I. E. Aronov, G. P. Berman, D. K. Campbell, and S. V. Dudiy, J. Phys.: Condens. Matter **9**, 5089 (1997).

[33] M. Büttiker, Phys. Rev. B **41**, 7906 (1990).

[34] H.-Z. Guo, J. Gao, and C. Lu, J. Appl. Phys. **105**, 124302 (2009).

[35] Y. M. Blanter, F. W. J. Hekking, and M. Büttiker, Phys. Rev. Lett. **81**, 1925 (1998).

[36] A. Prêtre, H. Thomas, and M. Büttiker, Phys. Rev. B **54**, 8130 (1996).

[37] M. H. Pedersen, S. A. van Langen, and M. Büttiker, Phys. Rev. B **57**, 1838 (1998).

[38] M. Misiorny, G. Fève, and J. Splettstoesser, Phys. Rev. B **97**, 075426 (2018).

[39] F. D. M. Haldane, J. Phys. C **14**, 2585 (1981).

[40] C. L. Kane and M. P. A. Fisher, Phys. Rev. Lett. **68**, 1220 (1992).

[41] K. Sasaoka, T. Yamamoto, S. Watanabe, and K. Shiraishi, Phys. Rev. B **84**, 125403 (2011).

[42] I. Safi and H. Saleur, Phys. Rev. Lett. **93**, 126602 (2004).

[43] S. Jezouin, M. Albert, F. D. Parmentier, A. Anthore, U. Gennser, A. Cavanna, I. Safi, and F. Pierre, Nat. Commun. **4**, 1802 (2013).

[44] M. Büttiker, in *Interacting Electrons in Nanostructures*, edited by R. Haug and H. Schoeller, Lecture Notes in Physics (Springer, Berlin/Heidelberg, 2001), pp. 149–164.

[45] B. J. van Wees, L. P. Kouwenhoven, E. M. M. Willems, C. J. P. M. Harmans, J. E. Mooij, H. van Houten, C. W. J. Beenakker, J. G. Williamson, and C. T. Foxon, Phys. Rev. B **43**, 12431 (1991).

[46] J. M. Caridad, S. R. Power, M. R. Lotz, A. A. Shylau, J. D. Thomsen, L. Gammelgaard, T. J. Booth, A.-P. Jauho, and P. Bøggild, Nat. Commun. **9**, 659 (2018).

[47] V. T. Renard, O. A. Tkachenko, V. A. Tkachenko, T. Ota, N. Kumada, J.-C. Portal, and Y. Hirayama, Phys. Rev. Lett. **100**, 186801 (2008).

[48] M. G. Prokudina, S. Ludwig, V. Pellegrini, L. Sorba, G. Biasiol, and V. S. Khrapai, Phys. Rev. Lett. **112**, 216402 (2014).

[49] S. Ilani, L. A. K. Donev, M. Kindermann, and P. L. McEuen, Nat. Phys. **2**, 687 (2006).

[50] L. I. Glazman, I. M. Ruzin, and B. I. Shklovskii, Phys. Rev. B **45**, 8454 (1992).

[51] M. M. Fogler, Phys. Rev. Lett. **94**, 056405 (2005).

[52] M. Hashisaka, N. Hiyama, T. Akiho, K. Muraki, and T. Fujisawa, Nat. Phys. **13**, 559 (2017).

[53] P. W. Brouwer and M. Büttiker, Europhys. Lett. **37**, 441 (1997).

[54] T. Müller, R. Thomale, B. Trauzettel, E. Bocquillon, and O. Kashuba, Phys. Rev. B **95**, 245114 (2017).

[55] D. H. Schimmel, B. Bruognolo, and J. von Delft, Phys. Rev. Lett. **119**, 196401 (2017).

[56] I. Gurman, R. Sabo, M. Heiblum, V. Umansky, and D. Mahalu, Phys. Rev. B **93**, 121412(R) (2016).

[57] A. Y. Alekseev and V. V. Cheianov, Phys. Rev. B **57**, 6834(R) (1998).